energies

Article

Numerical Modeling of the Steam Chamber Ramp-Up Phase in Steam-Assisted Gravity Drainage

Dongqi Ji [1,2], Jiacheng Xu [3], Xue Lyu [4], Zhiping Li [1,2,*] and Jie Zhan [5]

[1] School of Energy Resources, China University of Geosciences (Beijing), Beijing 100083, China; dongqi.ji@cugb.edu.cn
[2] Beijing Key Laboratory of Unconventional Natural Gas Geological Evaluation and Development Engineering, China University of Geosciences (Beijing), Beijing 100083, China
[3] Research Institute of Petroleum Exploration and Development, Beijing 100083, China; xujiacheng@petrochina.com.cn
[4] Sino-Pipeline International Company Limited, Beijing 102206, China; xue.lv@cnpc.com.cn
[5] School of Petroleum Engineering, Xi'an Shiyou University, Xi'an 710065, China; zhanjie@xsyu.edu.cn
* Correspondence: lzp_cugb@163.com; Tel.: +86-10-82320690

Abstract: Due to the critical nature of the ramp-up phase of an efficient steam-assisted gravity drainage (SAGD) process, it is important to understand the physics of the steam chamber ramp-up phase in order to improve SAGD production performance. In conventional numerical simulation models, the dynamics of the steam chamber ramp-up phase are not fully resolved because of unclear steam–oil–water interactions during the vertical growth of the steam chamber and how its state changes as the reservoir parameters vary. This work provides an efficient approach for the numerical modeling of the steam chamber ramp-up phase in an SAGD operation. The steam chamber ramp-up phase was fully examined through the consideration of the effects of the temperature-dependent oil–water–gas multiphase flow system and the vertical countercurrent flow. The simulation results revealed that for the large temperature gradient of the mobile oil zone at the edge of the steam chamber, a delicate temperature-dependent multiphase flow system was essential for the reliable estimation of the SAGD ramp-up phase. The vertical countercurrent flows of oil–gas and oil–condensate were the dominant mechanisms over cocurrent flow, which significantly impacted the steam chamber ramp-up rate. The numerical model physically predicted the steam chamber ramp-up phase and could be used to efficiently compute a field-scale simulation using a dynamic gridding function that was based on a fine grid model.

Keywords: SAGD; steam chamber ramp-up; numerical simulation; dynamic gridding

Citation: Ji, D.; Xu, J.; Lyu, X.; Li, Z.; Zhan, J. Numerical Modeling of the Steam Chamber Ramp-Up Phase in Steam-Assisted Gravity Drainage. *Energies* **2022**, *15*, 2933. https://doi.org/10.3390/en15082933

Academic Editors: Daigang Wang, Junjian Li and Jalel Azaiez

Received: 16 March 2022
Accepted: 14 April 2022
Published: 16 April 2022

1. Introduction

In a typical SAGD operation, a pair of horizontal wells are utilized for the recovery of heavy oil or bitumen reservoirs. The production well is drilled 2 m above the bottom of the reservoir and the injection well is parallel to and 5 m above the production well [1–3]. Saturated steam is injected into the reservoir through the injection well to form a steam chamber within the reservoir. The steam flows inside the steam chamber and condenses at the edge of the steam chamber once it encounters the cool oil that is in the reservoir. As the heat transfers from the hot steam chamber to the surrounding cold formations, heavy oil or bitumen is mobilized under the high temperature. Therefore, the heated oil and condensate flow downward into the production well due to gravity [4,5]. The steam chamber gradually expands with the developing evacuated space that is caused by the steam injection [6].

Due to the intrinsic impact of the expansion of an SAGD steam chamber on its production performance, modeling and understanding the growth of the steam chamber have been important research topics [7]. During a typical SAGD process, results from laboratory experiments [1,8] and observations from Underground Test Facility (UTF) field applications [9] have demonstrated that the steam chamber grows in three stages: ramp-up, lateral spreading and wind down. In the early stage of SAGD, which is referred to as the ramp-up phase, the steam chamber mainly grows in a vertical direction [10]. In the analysis of field applications data, it has been summarized that most SAGD ramp-up phases are completed in one to two years [11]. Additionally, analytical calculations have concluded that the ramp-up phase is closely related to the instability of the steam–condensate–oil front at the top of the chamber [12]. Therefore, it is important to have a reliable estimation of the performance of the ramp-up phase [9,13] through the consideration of the steam–oil–water interaction.

Analytical and numerical models have been proposed for the prediction of the SAGD ramp-up phase and the corresponding steam chamber evolution process. It is commonly assumed that the growth of a steam chamber solely occurs in the vertical direction during the ramp-up phase [1,14]. However, these models cannot predict the dynamic characteristics of the real inclined edge of a steam chamber during the ramp-up phase, which simultaneously grows in upward and lateral directions [15,16]. Recently, the use of the flat top of a steam chamber in an analytical model has been assumed to obtain an estimation of the ramp-up phase [13]. Further analytical models assume the steam chamber to be an inverted triangle that rises at a constant angle from the bottom production well to the reservoir overburden [17]. One particular concern is that there is an instable condensate–oil interface at the top of the steam chamber [18].

In the previous models of the steam chamber ramp-up phase, some critical reservoir properties, such as the input parameters, have not been appropriately included. In the SAGD process, there is a large temperature gradient in the oil drainage zone at the edge of a steam chamber between the steam temperature and the original reservoir temperature. The behavior of the multiphase fluid flow, which is estimated using relative permeabilities, is sensitive to the temperature gradient in this oil drainage zone and is essential to be considered [19]. Both experimental and mathematical studies have reported that in the process of thermal oil recovery, significant effects of temperature-dependent oil–water relative permeability have been observed on oil production [20–30]. Some models have been proposed for the representation of temperature-dependent relative permeabilities [20,30–32]. Between the original reservoir temperature and the saturated steam temperature, the water relative permeability endpoint can increase by two orders of magnitude [33] and the oil relative permeability endpoint can also alternate [19,27]. Further investigations on the temperature-dependent liquid–gas relative permeabilities in heavy oil systems have also been conducted. Experimental results have shown that the oil relative permeability changes slightly and the gas relative permeability increases gradually with the increase in temperature from 54 to 150 °C [34]. Although it is known that the oil–water–gas relative permeability system changes with temperature, the isothermal relative permeability curves are often used to predict the multiphase flow regardless of the large temperature range that is involved in the SAGD process [35]. Therefore, this isothermal relative permeability system can lead to significant uncertainties when applied in thermal oil recovery process estimations [24].

During an SAGD ramp-up phase, a lighter steam penetrates the heavier heavy oil or bitumen formation above it due to the buoyance effect, which leads to the erosion of the top of the steam chamber [4,8,36]. A critical uniqueness has been proposed in that the performance of SAGD relies on the vertically moving fluids in the countercurrent flows [37]. The comparisons between co- and countercurrent flows have been analyzed using both experiments and mathematical computations [38–41]. Due to the differences in phase flow velocities, momentum transfer accelerates the slower fluid flow and decelerates the faster moving fluids when the fluids are moving in a cocurrent manner. Correspondingly, when the fluids are moving in a countercurrent manner, both fluids are decelerated [41–44]. Review work that was based on these results has proposed the following concern: both co- and countercurrent flows occur at the steam interface and the combination of co- and countercurrent flows could have a profound impact on the ramp-up phase [45]. Hence, flow potential-dependent relative permeabilities that are caused by the combination of co- and countercurrent flows have to be considered in the modeling of an SAGD ramp-up phase, which has not yet been fully resolved.

Numerical reservoir simulation has always been a powerful tool for the estimation of the physics of SAGD processes. However, the accuracy, efficiency and robustness of the simulation highly depends on the input parameters and computation methodology. Notwithstanding the extensive research studies that have been conducted on the techniques for the estimation of the steam chamber ramp-up phase in SAGD, the models are not capable of adequately capturing the physics of the vertical ramp-up phase or estimating the oil production performance. Thus, it is difficult to account for complexities, such as the temperature-dependent oil–water–gas relative permeabilities, the combination of vertical co- and countercurrent flows, initial water saturation variations and their effects on steam chamber ramp-up phase performance. In order to obtain reliable simulation results, in contrast to previous simulation studies, the physical dynamic process of the steam chamber ramp-up phase was revealed in this study. The simulation effectively integrated the vertical steam chamber ramp-up physics and efficiently computed the process by applying the dynamic gridding algorithm in CMG STARS. As a result, this paper could provide a deeper understanding of the vertical steam chamber ramp-up mechanisms within the SAGD process.

2. Theory

In this work, a numerical model for governing the steam chamber ramp-up phase of an SAGD process was theorized, as shown in the schematic of a steam chamber cross-section in Figure 1. Below the top of the steam chamber, steam rises upward from the reservoir due to buoyancy effects as oil and condensate drain downward [4,15]. To capture the physics of the expansion of a steam chamber during the ramp-up phase, a fine grid reservoir model was applied. The model integrated the temperature-dependent oil–water–gas multiphase flow system and the vertical co- and countercurrent flows that are induced by the upward moving steam and downward moving heated oil and condensate. To efficiently accelerate the simulation, the dynamic gridding algorithm was optimized by dynamically reducing the total number of grids that were used in the model, depending on the specified trigger criterion.

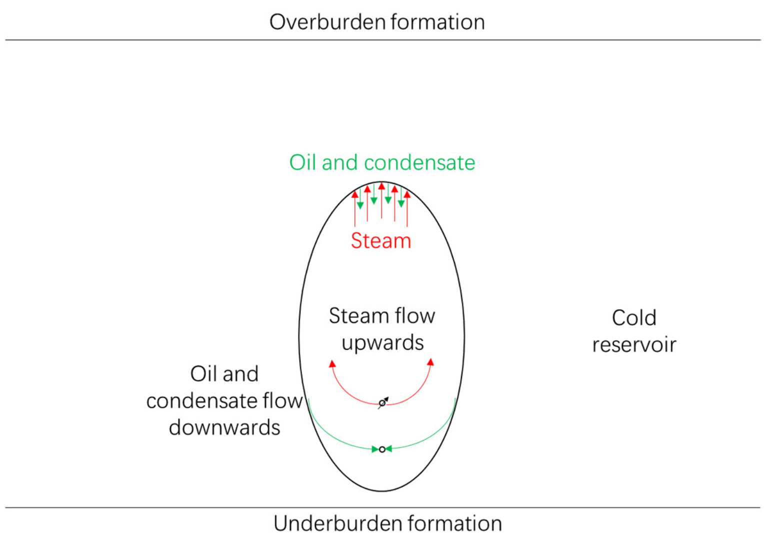

Figure 1. The cross-section of a steam chamber during the ramp-up phase of a typical SAGD operation.

2.1. Fine Grid Model

In the numerical reservoir simulation of the SAGD process, it was essential to apply sufficiently fine grids for the accurate estimation of the steam chamber [46]. Recent work on the effects of grid dimensions on thermal oil recovery simulation has further indicated that a fine grid system eliminates the impact of numerical diffusion on the numerical estimation, which is caused by the discretization in space and time [47]. In this work, a field-scale numerical simulation model with fine grids was built to investigate the multiphase fluid flow mechanisms and dynamic steam chamber expansion during the ramp-up phase of an SAGD process. A grid size sensitivity analysis that was based on the cumulative oil production comparison was also conducted to determine the appropriate grid size for the modeling of the target process.

2.2. Temperature-Dependent MultiPhase Flow

In recent years, many researchers have established correlations to express temperature-dependent oil–water relative permeability [32,48]. Mathematical analysis has proved that the Corey correlation can reliably predict temperature-dependent relative permeability curves [24,49]. The experimental data from the Athabasca bitumen and water system demonstrated that the generalized Corey relative permeability model, as shown below in Equations (1) and (2), could be employed to compute temperature-dependent oil and water relative permeability curves [19,27,29,30]:

$$k_{rw} = k_{rw}^0(T)\left(\frac{S_w - S_{wcon}(T)}{1 - S_{orw}(T) - S_{wcon}(T)}\right)^{N_w}, \tag{1}$$

$$k_{row} = k_{row}^0(T)\left(1 - \frac{S_w - S_{wcon}(T)}{1 - S_{orw}(T) - S_{wcon}(T)}\right)^{N_o}, \tag{2}$$

where $k_{rw}^0(T)$ is the water relative permeability endpoint in the oil–water system, $k_{ro}^0(T)$ is the oil relative permeability endpoint in the oil–water system, S_w is the water saturation, $S_{wcon}(T)$ is the connate water saturation, $S_{orw}(T)$ is the residual oil saturation, N_w is the water exponent and N_o is the oil exponent.

Four endpoints of a temperature-dependent oil–water relative permeability have been studied simultaneously in recent literature and the regressed correlations have been applied to estimate the dependence. Equations (3) and (4) were used to express the temperature-dependent connate water saturation and residual oil saturation of the Athabasca oil sands, respectively [27]:

$$S_{wcon} = 2.68 \times 10^{-4} T(K) - 0.0352, \tag{3}$$

$$S_{orw} = -0.419 \ln(T(K)) + 2.761, \tag{4}$$

The nonlinear trend curve of the oil endpoint relative permeability ($k_{ro}^0(T)$) was proposed according to the well-matched results of the experimental data, as shown in Equation (5), while the water endpoint relative permeability ($k_{rw}^0(T)$) was assumed to be a constant ($k_{rw}^0(T) = 1$). In addition, the water exponent (N_w) and oil exponent (N_o) were determined by fitting at 2.8 and 1.8, respectively [27], for the Athabasca oil sands.

$$k_{row}^0(T) = 0.4947 \ln(T(°\mathrm{C})) - 1.666, \tag{5}$$

The fitted Corey relative permeability model (Equations (6) and (7)) of the temperature-dependent liquid–gas relative permeabilities were also provided based on the simulation work of the Athabasca oil sands SAGD project, which has also been successfully integrated with the temperature-dependent oil–water relative permeability models [50,51].

$$k_{rg} = k_{rg}^0(T)\left(\frac{S_g - S_{gcon}(T)}{1 - S_{gcon}(T) - S_{org}(T) - S_{wcon}(T)}\right)^{N_g}, \tag{6}$$

$$k_{rog} = k_{rog}^{0}(T)\left(\frac{1 - S_g - S_{org} - S_{wcon}(T)}{1 - S_{gcon}(T) - S_{org}(T) - S_{wcon}(T)}\right)^{N_{og}}, \tag{7}$$

where, $k_{rg}^{0}(T)$ is the gas relative permeability endpoint in the liquid–gas system, $k_{rog}^{0}(T)$ is the liquid relative permeability endpoint in the liquid–gas system, S_g is the gas saturation, $S_{gcon}(T)$ is the connate gas saturation, $S_{org}(T)$ is the residual oil saturation in the liquid–gas system, N_g is the gas exponent and N_{og} is the liquid exponent.

The liquid endpoint relative permeability ($k_{rog}^{0}(T)$) equaled the oil endpoint relative permeability ($k_{row}^{0}(T)$). The temperature-dependent gas relative permeability endpoint ($k_{rg}^{0}(T)$), gas exponent (N_g) and liquid exponent (N_{og}) were also obtained using the regression method, as expressed by Equations (8)–(10), respectively:

$$k_{rg}^{0}(T) = -7.11 \times 10^{-7} T(°\mathrm{C})^2 + 2.267 \times 10^{-4} T(°\mathrm{C}) + 0.466, \tag{8}$$

$$N_g = -0.0018 \times T(°\mathrm{C}) + 1.1375, \tag{9}$$

$$N_{og} = 0.0153 \times T(°\mathrm{C}) - 0.2667, \tag{10}$$

2.3. Countercurrent Flow in the Vertical Direction

To simulate the process of the countercurrent flow, decreasing two-phase relative permeabilities have been demonstrated to be the most appropriate technique for estimation, according to the comparison of numerical results to experiment data [38]. In this technique, Corey-type equations are used to generate countercurrent flow relative permeability curves that are based on the corresponding cocurrent curves [41]. In this work, the countercurrent flow relative permeabilities were also generated according to the temperature-dependent cocurrent relative permeability curves by decreasing the relative permeability endpoints ($k_{rw}^{0}(T)$, $k_{row}^{0}(T)$, $k_{rg}^{0}(T)$ and $k_{rog}^{0}(T)$) to 50% [41]. The flow potential of each phase was dynamically tested and shifted between co- and countercurrent relative permeability curves in every region (every grid cell) during the simulation [52,53].

2.4. Dynamic Gridding

In a high-resolution numerical simulation, an entire reservoir model that is made up of fine grids can enhance the accuracy of the simulation, which results in a long computation time and, therefore, is impractical in a field-scale modeling [54]. Dynamic gridding is the methodology that is used to combine the local fine grids into groups and create relatively coarse grids that are controlled by a property gradient among the neighboring fine grids. On the contrary, once the gradient is larger than the threshold, de-amalgamation is executed and the local fine grids reappear [54,55]. Previous simulation work has demonstrated that dynamic gridding is an effective approach for accelerating computation by automatically adjusting the grid size and reducing computation time [54]. By comparing the simulation results from a fine grid model and a dynamic model, it was found that the temperature gradient is the best criterion to use to control the dynamic gridding in the thermal oil recovery process [54]. In this work, the commercial simulator CMG STARS was utilized for the dynamic gridding feature, in which both grid amalgamation and grid refinement were fully included [53]. The controlling parameters and threshold values that were used for the dynamic gridding application to capture the physics of the steam chamber ramp-up phase are examined in the next subsection.

3. Simulation Model

In this study, the proposed reservoir model represented the Athabasca oil sands in Alberta, Canada [56]. The commercial simulator CMG STARS, version 2020.10, which is a widely applied thermal oil recovery simulation tool, was used to generate the simulation model and perform the simulation computations [5,53]. This model included a horizontal pair of wells that were drilled at the bottom of the reservoir. To make the study on the cross-sectional steam chamber ramp-up phase more straightforward, a two-dimensional model was utilized [56]. The key assumptions and simplifications that were used to develop the proposed simulation model for evaluating the steam chamber ramp-up phase in SAGD operation are summarized as follows:

1. A homogeneous simulation model was used with averaged porosity, permeability, initial temperature and oil viscosity;
2. The bitumen that was deposited in the reservoir was single-component and dead without solution gas;
3. The fluids, such as water and bitumen were immiscible and Newtonian;
4. The effects of capillary pressure on fluid flow were neglected due to the high permeability.

The target reservoir had a deposition of 300 m, a thickness of 20 m and a width of 20 m, as shown in the schematic in Figure 2. The key reservoir properties are summarized in Table 1. The average reservoir porosity was 0.3 and the ratio of vertical permeability to horizontal permeability equaled 0.4 with a vertical permeability of 4 darcys. The initial oil saturation and temperature were 0.8 and 20 °C, respectively. The bitumen viscosity that was hosted under the initial reservoir condition was over 1 million cP [56]. To reduce the effects of numerical dispersion, the fine grids were used in both the lateral and vertical directions, which has been confirmed to be sufficient in the simulation of steam chamber expansion in SAGD [57]. The reservoir was modeled with a single 800 m long grid along the horizontal well. Prior to the SAGD production mode, pre-heating between the injection and production wells was established by the circulation of steam within the two wells, while fluid production was constrained by bottom hole pressure, which was equal to the original reservoir pressure [56]. Then, steam was introduced into the injection well at a pressure of 2200 kPa (217 °C) and a steam quality of 0.8. The production through the production well was constrained under a maximum steam production rate of 1 m^3/day (CWE) [10]. The reservoir simulation was run for 13 months of a steam chamber ramp-up phase [58].

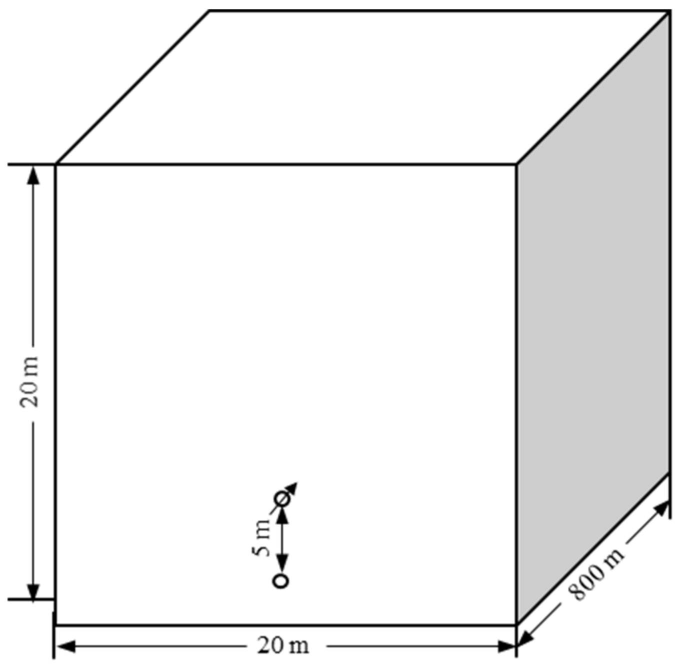

Figure 2. Schematic of the reservoir model used for the SAGD simulation.

Table 1. Key reservoir model parameters.

Items	Values
Depth to top of reservoir (reference depth), m	300
Net pay, m	20
Reference pressure, kPa	1300
Initial water saturation, %	20
Initial oil saturation, %	80
Initial reservoir temperature (reference temperature), °C	20
Horizontal absolute permeability, darcy	4.0
Vertical absolute permeability, darcy	1.6
Formation compressibility, 1/kPa	8.0×10^{-6}
Formation heat capacity, J/(m^3×°C)	2.35×10^{6}
Rock conductivity, J/(m×day×°C)	6.60×10^{5}
Water conductivity, J/(m×day×°C)	5.35×10^{4}
Oil conductivity, J/(m×day×°C)	1.25×10^{4}
Gas conductivity, J/(m×day×°C)	3200
Overburden/underburden volumetric heat capacity, J/(m^3×°C)	2.35×10^{5}
Oil viscosity, cp	$lnln(\mu) = -3.5738\ln(T(°C)) + 22.8379$

The temperature-dependent oil-water-gas multiphase flow system was expressed as the oil–water and liquid–gas relative permeability curves at varying temperatures. The relative permeability values of the Athabasca oil sands were estimated using Equations (1)–(10) and the corresponding curves were plotted in the temperature range of 20 to 220 °C, as shown in Figure 3. Figure 3 shows the results that have been published in the literature, which demonstrate that the reservoir wettability tends to more water-wet [29] and gas mobility increases with the increase in temperature [34].

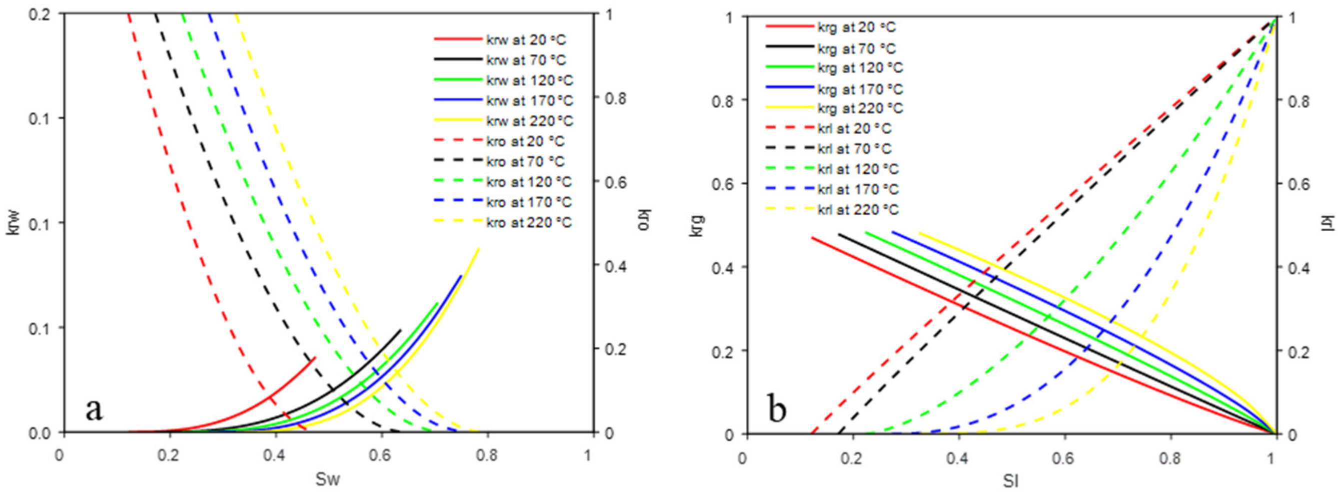

Figure 3. Temperature-dependent relative permeabilities of the Athabasca oil sands: (**a**) oil–water relative permeability curves and (**b**) liquid–gas relative permeability curves.

In the representation of the countercurrent flow relative permeability curves, cocurrent relative permeability curves were used as the reference and the endpoints of these curves were modified [38]. In all simulation scenarios, the relative permeabilities of the countercurrent flow were fixed by manually reducing the relative permeability endpoints in Equations (1), (2), (6) and (7) [59]. Figure 4 shows the oil–water and liquid–gas two-phase relative permeability curves when each phase relative permeability was reduced to 50% and the co- and countercurrent relative permeabilities were fixed at 220 °C [41].

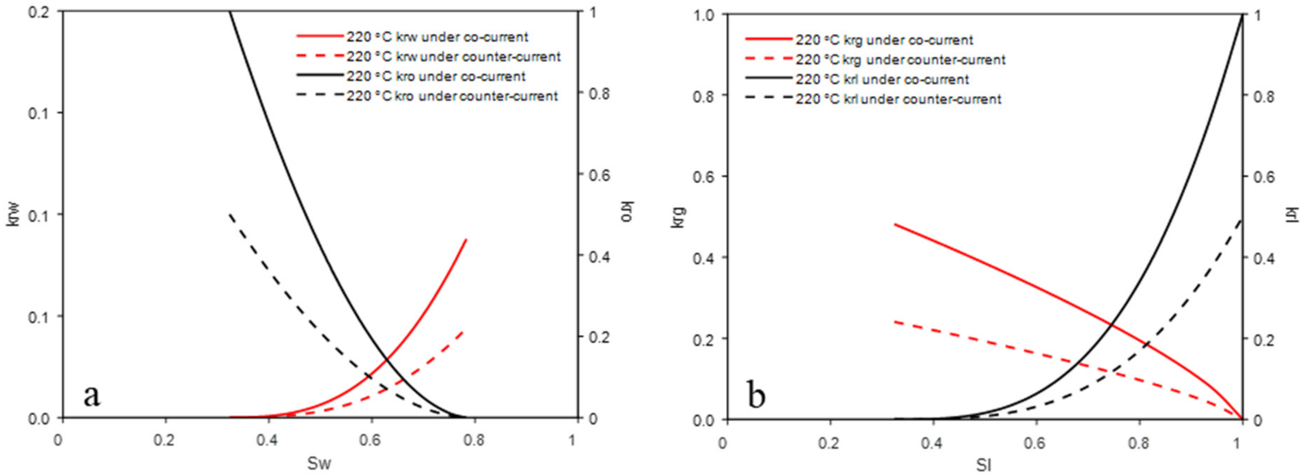

Figure 4. Co- and countercurrent relative permeabilities at 220 °C: (**a**) oil–water relative permeability curves and (**b**) liquid–gas relative permeability curves.

4. Model Validation

To obtain a reliable and robust simulation model, the numerical scheme was validated using four steps: reservoir width, grid size, dynamic gridding parameters and comparison to field performance.

4.1. Effects of Reservoir Width on Oil Production

Due to the simultaneous vertical and lateral growth of the steam chamber during an SAGD ramp-up phase [15,16], the reservoir width selection for the modeling process impacted the simulation performance. On one hand, when the reservoir was narrow, the early touching between the steam chamber and the side boundaries of the model impaired the accurate estimation of the vertical ramp-up phase. On the other hand, although a wide reservoir model could estimate the ramp-up phase accurately, the large number of grids on both sides of the model caused unnecessary additional computation time. Three reservoir widths of 15 m, 20 m and 25 m were simulated and compared to the results of the cumulative oil production curves that are plotted in Figure 5. During the comparison of the curves, it was found that the reservoir with a width of 20 m showed an excellent agreement with the larger reservoir width of 25 m. However, the narrow reservoir width of 15 m overestimated the oil production after 250 days due to the early touching between the steam chamber and the side boundaries. The narrow reservoir restricted later steam chamber growth and resulted in fast vertical steam chamber growth, as shown in the cross-sectional temperature distributions of the steam chamber at 330 days that are presented in Figure 6. To efficiently simulate the ramp-up phase, the 20 m reservoir width was selected for the following simulation work.

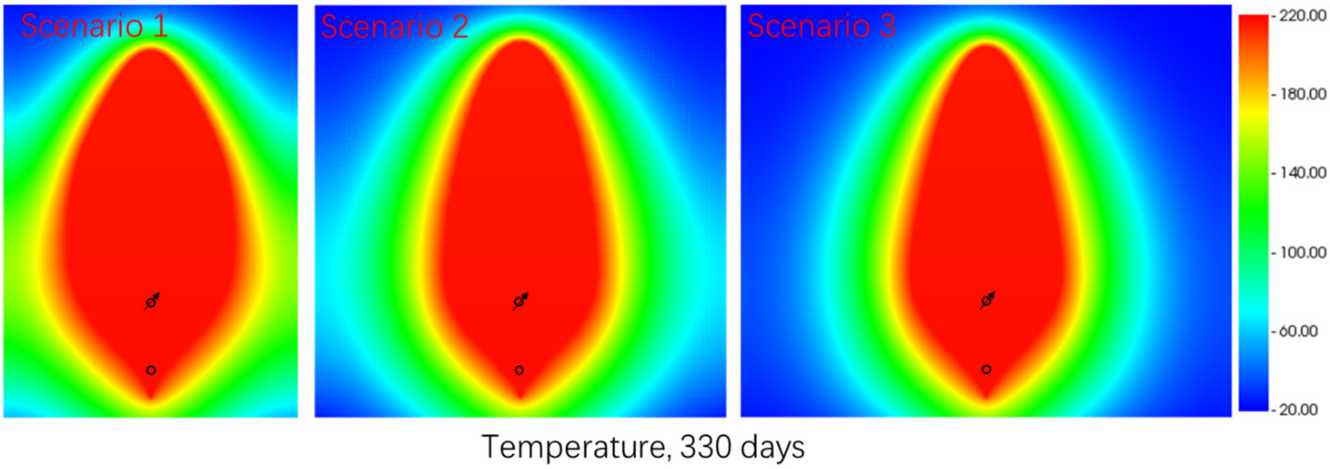

Figure 5. Cross-sectional temperature profiles of scenarios 1 to 3 under varying reservoir widths at 330 days.

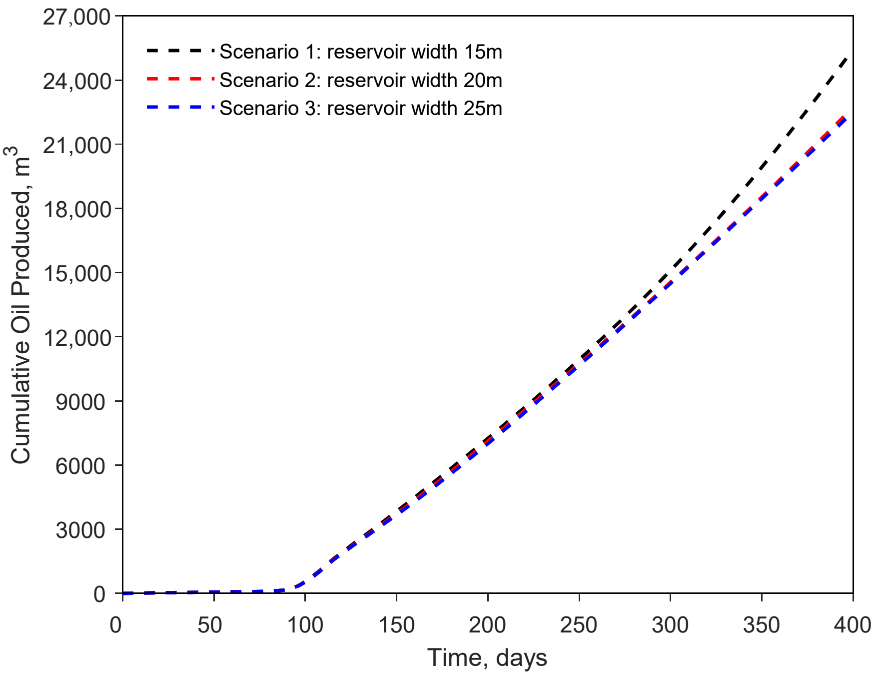

Figure 6. Cumulative oil production of scenarios 1 to 3 under varying reservoir widths.

4.2. Effects of Grid Size on Simulation Performance

Due to the significant effects of numerical diffusion/dispersion on the numerical simulation results, which was caused by the discretization in space and time [47], a sensitivity analysis on the impact of grid size on the SAGD ramp-up phase performance was conducted by comparing the cumulative oil production of varying grid sizes from 2.5 cm to 20 cm, as summarized in Table 2. The cumulative oil production by time, which was used as the grid size quality testing parameter [59], were plotted in curves, which are presented in Figure 7. From the comparison of the curves, it was observed that the large grid sizes (Scenario 5 and 6) accelerated the oil production rate because the large grid system overestimated the heat transfer, which is the dominant oil flow enhancement mechanism of SAGD [60]. It is also demonstrated that the grid size of 5.0 cm $\times$ 5.0 cm (scenario 2) produced a high accuracy with a good agreement with the results that were computed by the smaller grid size of 2.5 cm $\times$ 2.5 cm (scenario 4), while the computation time for the 2.5 cm grid size was much longer than that for the 5.0 cm grid size, as summarized in Table 3. By using fine grids, the effects of heat transfer on both thermal conductivity and convection were greater than the effects of the numerical diffusion/dispersion on the SAGD performance. As a consequence, the impact of numerical diffusion/dispersion on the numerically simulated steam chamber ramp-up phase could be neglected by applying the grid size of 5.0 cm × 5.0 cm. The findings were consistent with the results of previous studies in that millimeter-sized grids led to an accurate numerical diffusion/dispersion for the representation of the physical process [47]. Thus, to obtain an efficient simulation model, the grid size of 5.0 cm × 5.0 cm (scenario 2) was chosen as the base grid size. Furthermore, the grids (5.0 cm × 5.0 cm) that were used in this work were finer than the relatively coarse grids (20 cm × 20 cm) that are used in simple SAGD models [56] and in situ combustion models [47], in which isothermal relative permeability curves are used when neglecting the impact of the countercurrent flows. Thus, the temperature-dependent oil–water–gas multiphase flows and buoyancy-induced countercurrent flows required fine grids for an effective numerical simulation.

Table 2. Scenarios demonstrating the impact of reservoir width on SAGD ramp-up phase.

Case	Description
Scenario 1	Reservoir width = 15 m
Scenario 2	Reservoir width = 20 m
Scenario 3	Reservoir width = 25 m

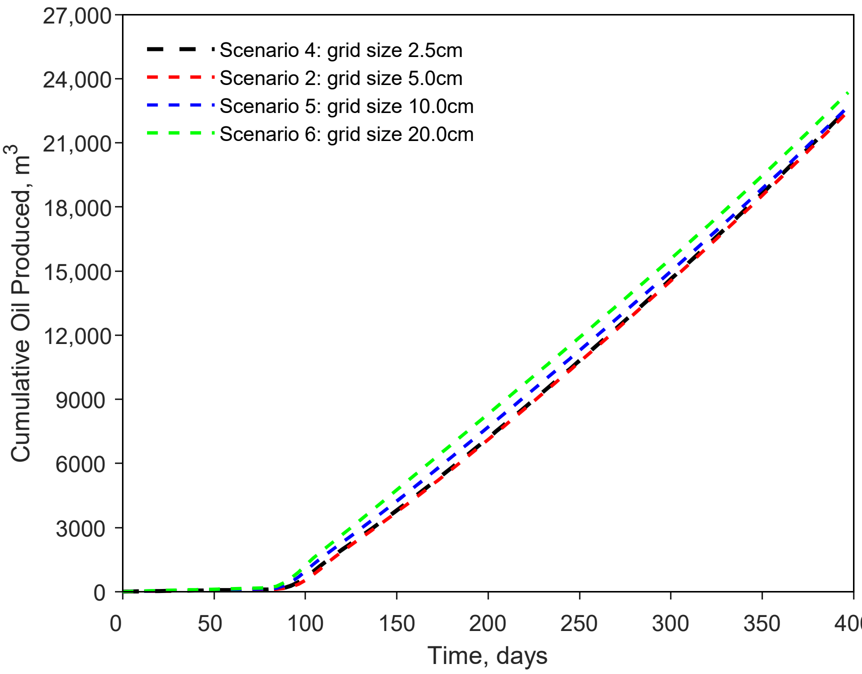

Figure 7. Cumulative oil production of scenarios 2, 4, 5 and 6 under varying reservoir model grids.

Table 3. Summary of scenarios for grid size selection.

Case	Description
Scenario 2	Grid size = 5.0 cm × 5.0 cm
Scenario 4	Grid size = 2.5 cm × 2.5 cm
Scenario 5	Grid size = 10 cm × 10 cm
Scenario 6	Grid size = 20 cm × 20 cm

4.3. Dynamic Gridding and Numerical Convergence

In this work, dynamic gridding was applied to overcome the issue of long computation time that is required for fine grid SAGD simulation. In the dynamic gridding scenarios, once the amalgamation was activated, the fine grids were locally combined to create coarse grids by monitoring the threshold value, which was the temperature difference between the neighboring grids [47]. Otherwise, the de-amalgamation was activated and the coarse grids were split into fine grids when the temperature difference was less than the threshold value. The simulation results from scenario 2 were used as the reference for the evaluation of the dynamic gridding parameters. Four scenarios (summarized in Table 4) were generated to examine the effects of various trigger temperatures on the simulation results.

In this work, a ten-core personal workstation (3.7 GHz processor) was used to perform the simulations. Figure 8 presents the temperature and oil saturation distributions of both scenario 2 and scenario 8 at 150 days, 240 days and 330 days. Further curves that demonstrate the cumulative oil production of the scenarios are shown in Figure 9. In scenario 8, fine grids (5.0 cm × 5.0 cm) covered the mobile oil region (as shown in the refined grids), while coarse grid blocks (25 cm × 25 cm) were generated inside the steam chamber and cold oil reservoir regions. Once the mobile oil region passed the threshold, the fine grids were combined into coarse grids behind the mobile oil region as time went on. After an abundance of sensitivity analyses, it was found that the temperature gradient that was used in scenario 8 (5 °C) had an excellent agreement with scenario 2, both in terms of the temperature distributions and cumulative oil production, as well as a reduced computation time (from 8 h 57 min to 2 h 1 min). Thus, according to the comparison of property distribution and oil production, the dynamic grid model could deliver a good representation of the fine grid model.

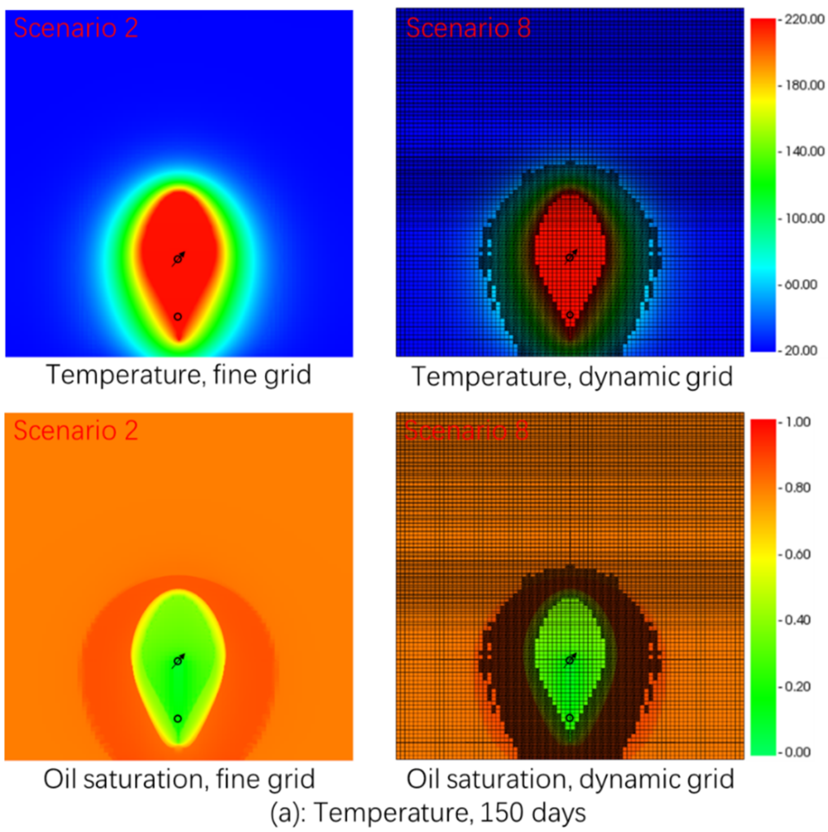

Figure 8. *Cont.*

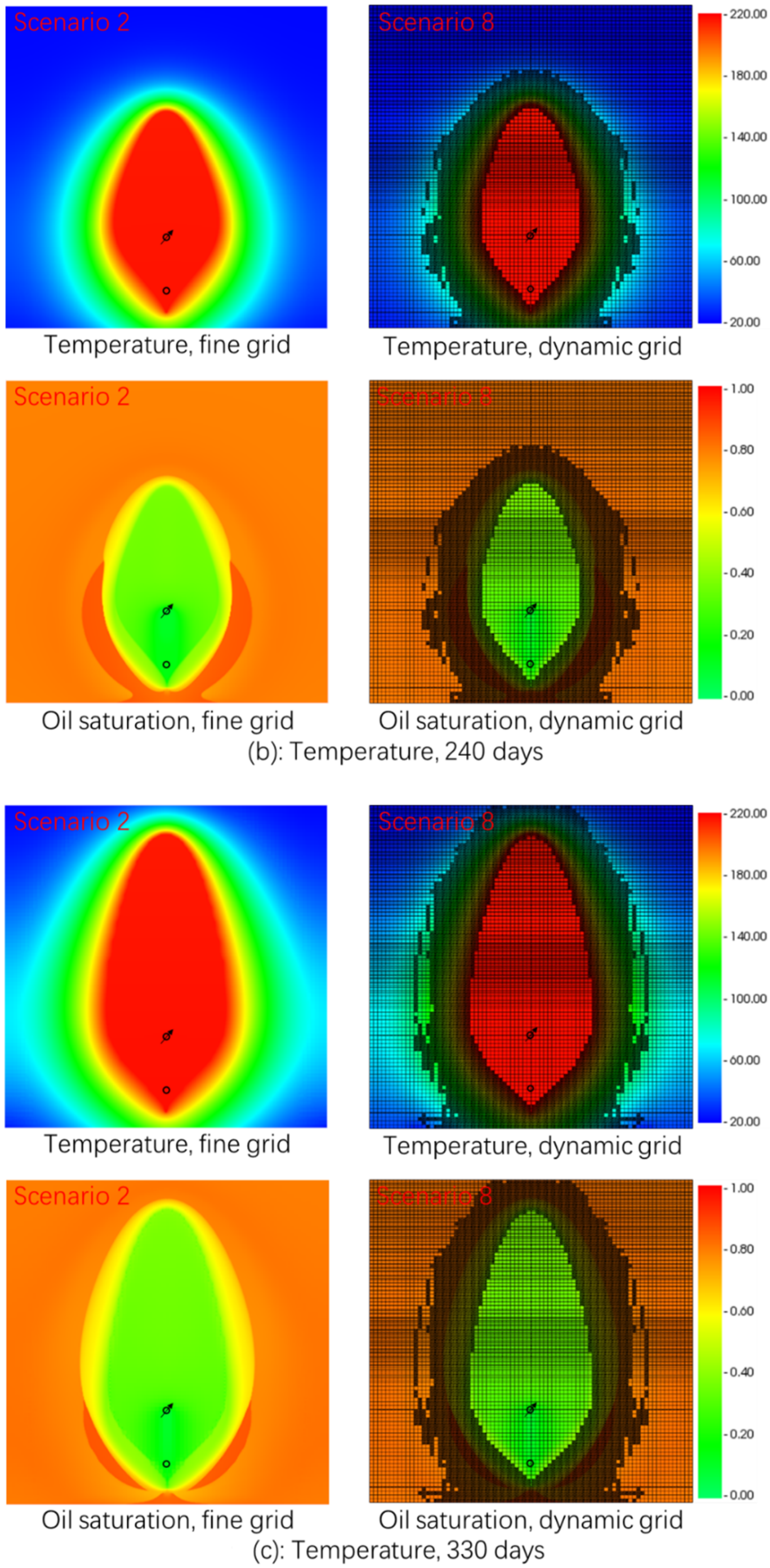

Figure 8. Cross-sectional temperature and oil saturation distributions of scenarios 2 and 8 at (**a**) 150 days, (**b**) 240 days and (**c**) 330 days.

Table 4. Cases of fine grid and dynamic grid scenarios.

Case	Description	Dynamic Grid Temperature Gradient	Average Timestep	Average Iterations	Simulation Time
Scenario 2	Fine grids; dimension = 5.0 cm × 5.0 cm	-	3×10^{-2} days	3	8 h 57 min
Scenario 7	Dynamic grids; amalgamation dimension = 25 cm × 25 cm	2 °C	5×10^{-2} days	2	3 h 16 min
Scenario 8	Dynamic grids; amalgamation dimension = 25 cm × 25 cm	5 °C	5×10^{-2} days	2	2 h 1min
Scenario 9	Dynamic grids; amalgamation dimension = 25 cm × 25 cm	10 °C	5×10^{-2} days	2	0 h 52 min

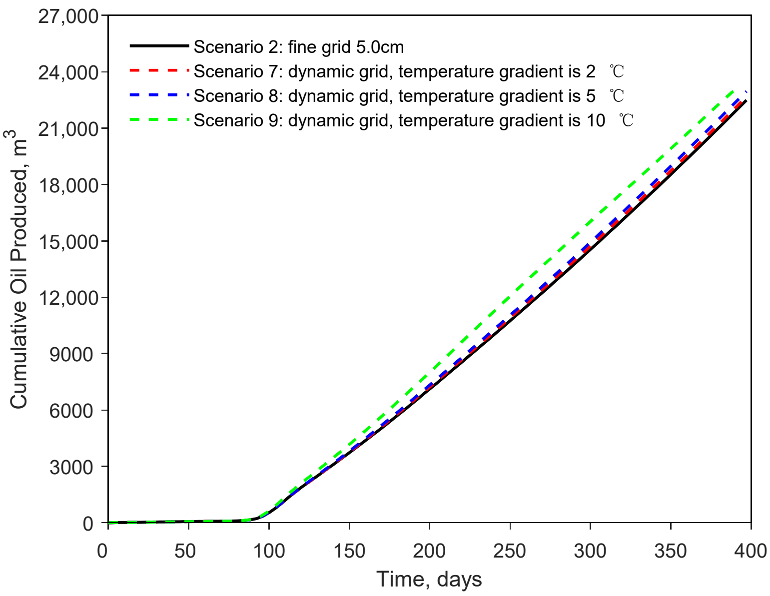

Figure 9. Cumulative oil production of scenarios 2, 7, 8 and 9 under the application of dynamic gridding.

As the steam chamber ramp-up phase involves complex flow behavior, which is temperature- and flow direction-dependent, an adaptive implicit numerical method using CMG STARS was applied to solve the strongly nonlinear system and enable efficient computation convergence. The automatically adjusted timestep size was utilized to facilitate convergence, in which the timestep size was appropriately increased after fast convergence and decreased when the iteration number exceeded the pre-set maximum level [53]. As shown in Table 4, the average timestep of scenario 2 without dynamic grids fluctuated around 2×10^{-2} days, while the average timestep increased to 5×10^{-2} days for scenario 8 under the application of dynamic grids. The average iteration number in each timestep also decreased from 3 to 2 after the application of dynamic grids in scenario 8. Thus, the proposed dynamic gridding model for the simulation of the steam chamber ramp-up phase was efficient in enlarging the average timestep and decreasing the number of iterations.

4.4. Comparison to Field Data

In this section, as well as the validation of the simulation parameters, the proposed simulation model is further validated against the Athabasca oil sands field observations of the Jackfish 1, Pad A SAGD project [61]. In the published literature, the Jackfish 1 SAGD project is located 150 km south of the city of Fort McMurray and has the same geological information of Athabasca oil sands deposit [61]. In the simulation model, the average reservoir properties of the Athabasca oil sands were used to represent the Jackfish 1 SAGD simulation, as shown in Table 1. In addition, due to the lack of operational details for the field project, the curves of the normalized cumulative oil production ($\frac{cumulative\ oil\ production}{cumulative\ oil\ production\ at\ 365\ \text{days}}$), which was a dimensionless parameter, versus time were plotted, as shown in Figure 10. The good agreement between the results of scenario 8 and those of the field project further demonstrated the validity of the generated simulation model for the estimation of the steam chamber ramp-up phase of the SAGD process in the Athabasca oil sands.

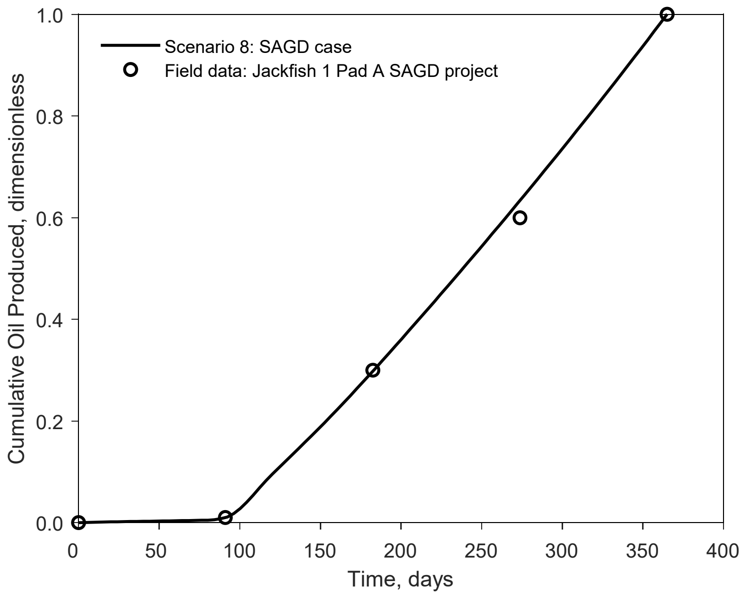

Figure 10. Comparison of the cumulative oil production results of simulation scenario 8 and the Jackfish 1, Pad A (Athabasca oil sands) SAGD project.

As a summary of the model validation, the generated numerical model provided reasonable predictions of the SAGD ramp-up phase, which could be designed to estimate the primary physics of the vertical growth of the steam chamber ramp-up phase and export a variety of outputs.

5. Results and Discussions

In this section, further simulation results and discussions are provided to obtain a deeper understanding of the SAGD ramp-up phase, based on the proposed model.

5.1. Characteristics of the Steam Chamber Ramp-Up Phase of the SAGD Process

Figure 11 depicts the process of an SAGD ramp-up phase that was based on the simulation results of scenario 8. In the left-hand column, the temperature distributions in the cross-section are shown at 150 days, 240 days and 330 days. The geometries of the growth of the steam chamber that were represented by the temperature distributions demonstrated the conclusion that the steam chamber grew upward and outward simultaneously during the ramp-up phase [15,16]. Correspondingly, a reference line (the dashed line shown in Figure 11, left-hand column) from the injection well to the top of the reservoir was selected and the relevant properties were plotted along that reference line, as shown in the right-hand column of Figure 11. The curves for the temperature and the gas, oil and water vertical flow velocities were also plotted and analyzed. The dashed line in the right-hand column separates the reservoir into two zones: the steam chamber and outside the steam chamber. The results revealed that in the steam chamber, as the hot steam came into contact with the cold oil, the steam condensed and the oil was mobilized by the high temperature. Then, the oil and condensate flowed downward (positive velocities) and the gas flowed upward (negative velocity) throughout the whole ramp-up phase. Thus, the countercurrent flows of steam–condensate and steam–oil occurred inside the steam chamber. Outside the steam chamber, both the oil and condensate flowed downward in a cocurrent manner without the existence of steam, due to the steam condensation.

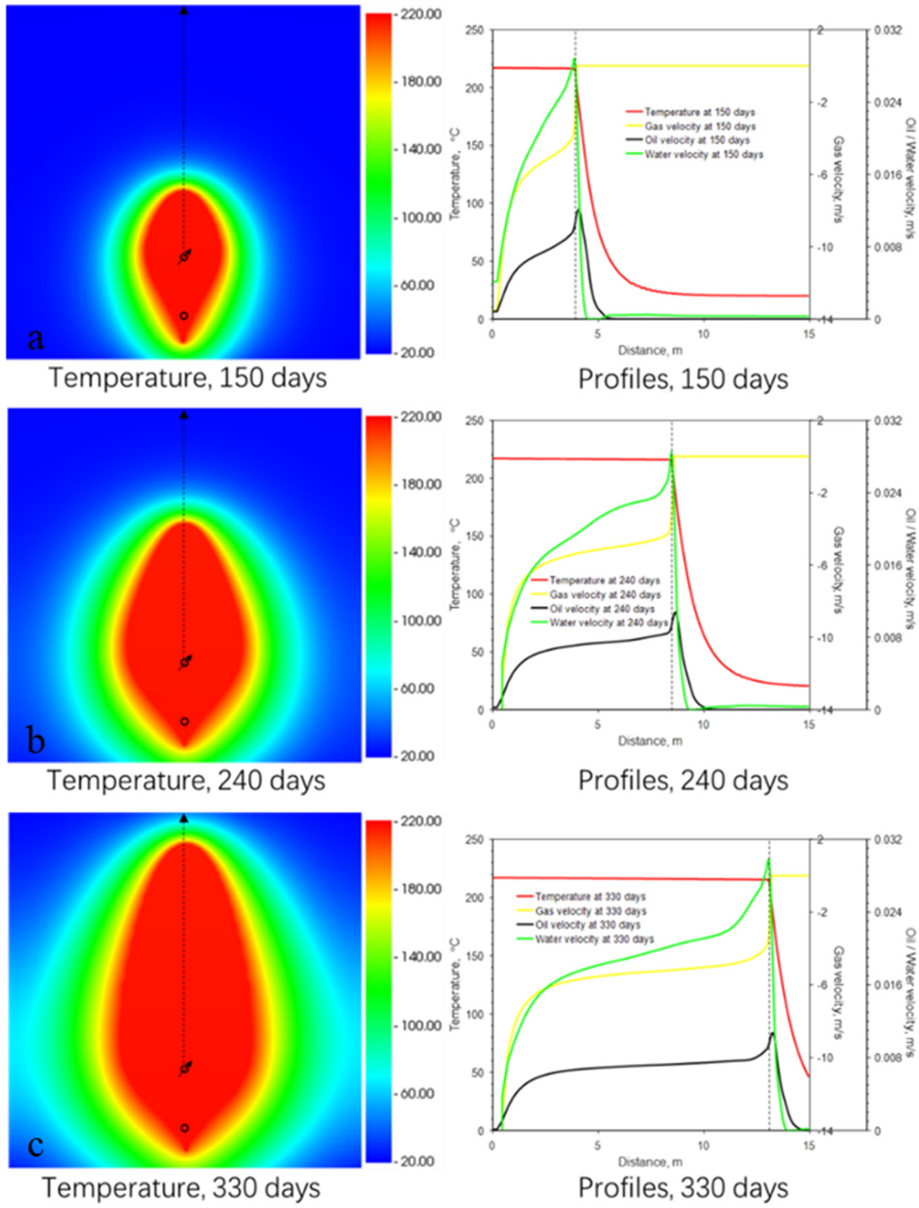

Figure 11. Characteristics of the steam chamber ramp-up phase at (**a**) 150 days, (**b**) 240 days and (**c**) 330 days: (left) cross-sectional temperature distributions; (right) temperature and the vertical flow velocities of gas, water and oil along the line from the injection well to the top of the reservoir.

5.2. Temperature-Dependent Relative Permeabilities and CounterCurrent Flow

Scenarios concerning the impact of the temperature-dependent multiphase flow and vertical countercurrent flow were computed and the corresponding results were analyzed. In Table 5, the relevant scenarios are summarized. Scenario 8 was the reference case, which integrated the temperature-dependent relative permeabilities and vertical countercurrent flows. To study the effects of temperature on the multiphase flow, scenarios 10 and 12 used an isothermal relative permeability system at the same temperature as the saturated steam. In scenarios 11 and 12, the vertical countercurrent flow was neglected by removing the countercurrent flow relative permeabilities, as shown in the curves in Figure 4.

Table 5. Scenarios of temperature-dependent relative permeabilities and countercurrent flow.

Case	Description
Scenario 8	Temperature-dependent relative permeabilities and countercurrent flow
Scenario 10	Temperature-independent relative permeabilities and countercurrent flow
Scenario 11	Temperature-dependent relative permeabilities and cocurrent flow
Scenario 12	Temperature-independent relative permeabilities and cocurrent flow

The cross-sectional temperature distributions of the four scenarios are displayed in Figure 12 and the corresponding cumulative oil production curves are plotted in Figure 13. Scenarios 8 and 10 produced similar temperature distributions, whereas the isothermal relative permeability system in scenario 10 relatively overestimated the amount of oil production compared to scenario 8. In the comparison of scenarios 11 and 12, the temperature-dependent multiphase flow system also produced more oil. Thus, using the delicate temperature-dependent multiphase flow system was essential for the SAGD ramp-up phase simulation due to the significant temperature variation in the mobile oil region, which was caused by the steam injection. Further analysis between the countercurrent scenarios (8 and 10) and cocurrent scenarios (11 and 12) was also conducted. The countercurrent flow decreased the effects of the temperature-dependent multiphase flow on the steam chamber ramp-up phase by decreasing difference between the oil production of scenarios 8 and 10 and scenarios 11 and 12. Thus, the countercurrent flow had a relatively greater impact on the ramp-up phase performance than the temperature-dependent multiphase flow.

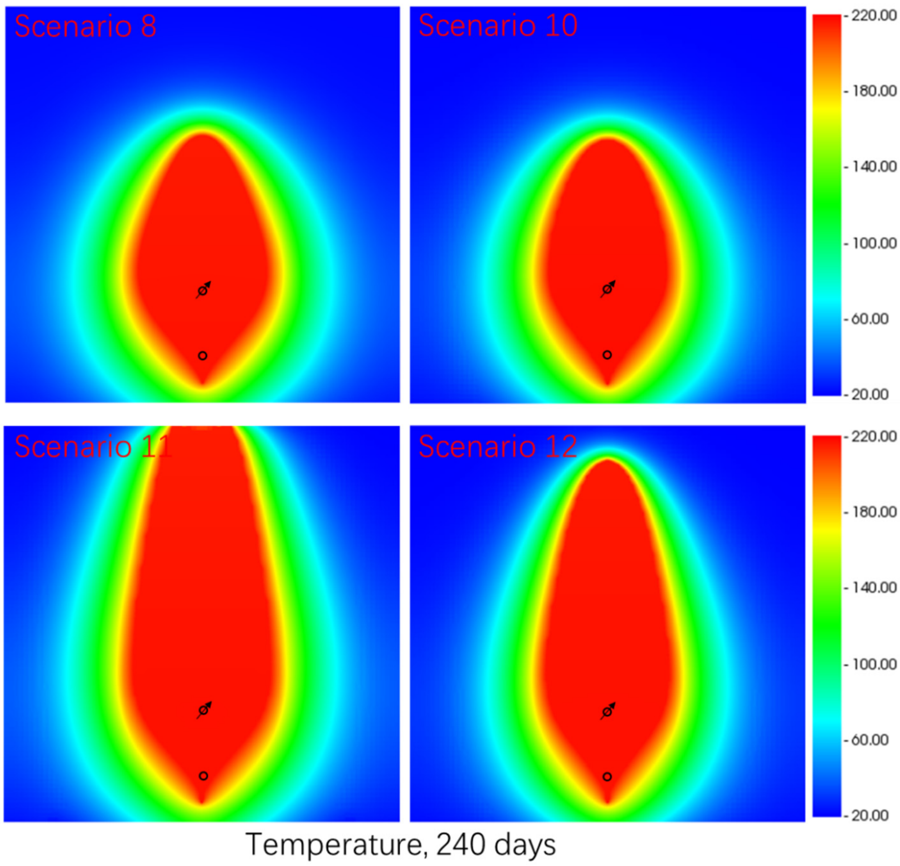

Figure 12. Cross-sectional temperature distributions of scenarios 8, 10, 11 and 12 under varying relative permeability settings.

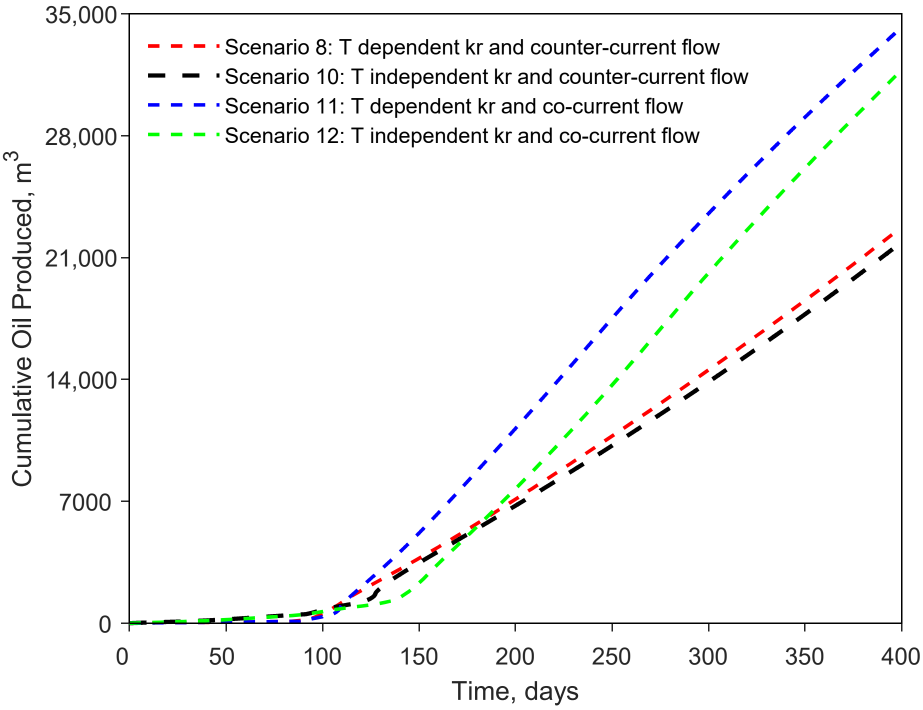

Figure 13. Cumulative oil production of scenarios 8, 10, 11 and 12 under varying relative permeability settings.

5.3. *Effects of Co- and Countercurrent Flows on the Ramp-Up Phase*

Using previous work on the estimation of countercurrent flow relative permeabilities through the decrease in the corresponding cocurrent flow relative permeabilities [41,59], the effects of the co- and countercurrent flows on the SAGD ramp-up phase were examined. Table 6 summarizes the scenarios for estimating the countercurrent relative permeability values using between 30% and 70% of the cocurrent flow relative permeability values, as well as a corresponding vertical permeability to horizontal permeability ratio (kv/kh) between 0.24 and 0.56. For example, in scenario 13, the countercurrent flow was reduced to 30% of that in scenario 8. In scenario 15, both the co- and countercurrent flow phases were decreased to 30% by reducing the vertical permeability compared to scenario 8. The simulation results for the cross-sectional temperature distributions and cumulative oil production curves are shown in Figure 14 and 15, respectively. A significant deceleration in the vertical growth of the steam chamber and a reduction in oil production were found with the decrease in both countercurrent flow relative permeability value and kv/kh ratio. These observations further demonstrated the assumption of the consistent deceleration of the ramp-up phase being caused by the vertical countercurrent flow during the SAGD ramp-up phase [17].

As discussions on the characteristics of the steam chamber ramp-up phase in the SAGD process have shown, steam–oil and steam–condensate countercurrent flows occur in the steam chamber and condensate–oil cocurrent flows may exist in the same region [62]. Further examinations of the impact of co- and countercurrent flows on oil production were conducted. In scenarios 15 and 16, the flow capacities of both co- and countercurrent flows were modified by varying the kv/kh ratio, whereas only the countercurrent flow was altered in scenarios 13 and 14. The acceleration of the steam chamber ramp-up phase by increasing vertical permeability was proven by the temperature distributions that are presented in Figure 14, which was similar to the effect of an increase in countercurrent relative permeability values. The curves for the cumulative oil production are plotted in Figure 15, including scenarios 8 and 13 to 16. Through the comparison of these curves, it was found that decreasing the countercurrent flow relative permeability values (only the countercurrent flow was decreased) had a similar effect to decreasing the vertical absolute oil reservoir permeability (both co- and countercurrent flows were reduced) on the oil production of the ramp-up phase, as can be seen from scenarios 13 and 15 and scenarios 14 and 16. In other words, the countercurrent flow was the dominant multiphase flow mechanism for the vertical growth of the SAGD ramp-up phase.

Table 6. Scenarios of modified countercurrent relative permeabilities and kv/kh ratios.

Case	Description
Scenario 8	Estimating countercurrent relative permeability by decreasing cocurrent relative permeability to 50%; kv/kh = 0.50
Scenario 13	Estimating countercurrent relative permeability by decreasing cocurrent relative permeability to 30%; kv/kh = 0.50
Scenario 14	Estimating countercurrent relative permeability by decreasing cocurrent relative permeability to 70%; kv/kh = 0.50
Scenario 15	Estimating countercurrent relative permeability by decreasing cocurrent relative permeability to 50%; kv/kh = 0.24
Scenario 16	Estimating countercurrent relative permeability by decreasing cocurrent relative permeability to 50%; kv/kh = 0.56

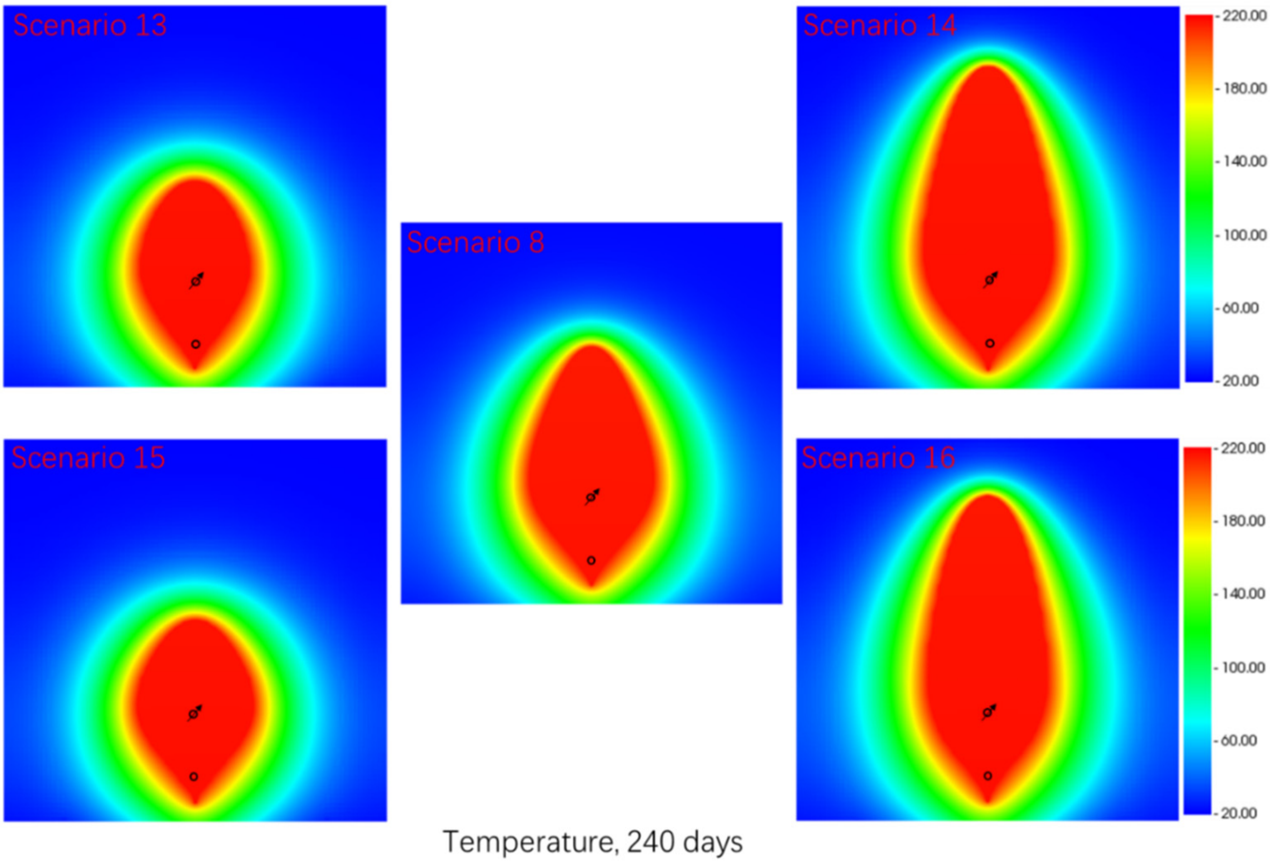

Figure 14. Cross-sectional temperature distributions of scenarios 8, 13, 14, 15 and 16 under varying countercurrent relative permeability values and vertical permeabilities using kv/kh ratios.

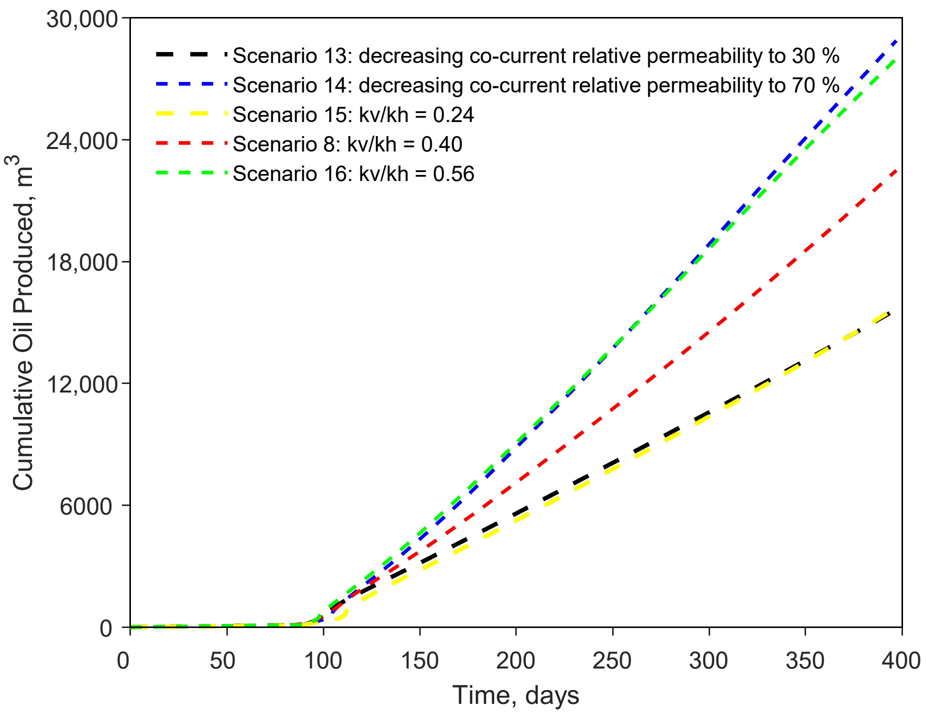

Figure 15. Cumulative oil production of scenarios 8, 13, 14, 15 and 16 under varying countercurrent relative permeability values and vertical permeabilities using kv/kh ratios.

5.4. Effects of Initial Water Mobility on the Steam Chamber Ramp-Up Phase

Laboratory experiment results have demonstrated that the initial water is mobile when the saturation is above 7% at room temperature [63]. The mobile water outside the steam chamber boundary could significantly impact the growth of the steam chamber [64]. In this work, the effects of the initial water mobility on the SAGD ramp-up phase performance were examined by altering the initial water saturation. Table 7 presents the scenarios with initial water saturation values ranging from 0.1 to 0.3. The corresponding cross-sectional temperature distributions are shown in Figure 16 and the cumulative oil production curves are plotted in Figure 17. The comparison of scenarios 8 and 17 revealed that the rate of steam chamber growth was almost unchanged when the initial oil saturation increased from 0.1 to 0.2. In contrast, there was significantly rapid steam chamber growth in scenario 18 with the initial water saturation of 0.3. The amount of temperature-dependent connate water saturation that was in the representation of the water saturation endpoint in Figure 3 confirmed that under at the temperature of the injected steam (217 °C), initial water saturation was mobilized when the saturation was over 0.28. As a result, the convective flow of mobile water in the oil reservoir accelerated the heat transfer outside the steam chamber boundary. Thus, the simulation results were consistent with those from previous experiments in terms of the tendency of a high initial water saturation value enabling a faster steam chamber ramp-up phase compared to a low initial water saturation value [56]. The curves of the cumulative oil production that are presented in Figure 17 demonstrate that a lower amount of oil was recovered when the initial water saturation was high. Although there was a large area of reservoir that was swept by steam in scenario 18, under high initial water saturation conditions, the low initial oil saturation counteracted the large steam chamber growth and decreased the total amount of oil that was produced.

Table 7. Scenarios of varying initial water saturation.

Case	Description
Scenario 8	Initial water saturation = 0.20
Scenario 17	Initial water saturation = 0.10
Scenario 18	Initial water saturation = 0.30

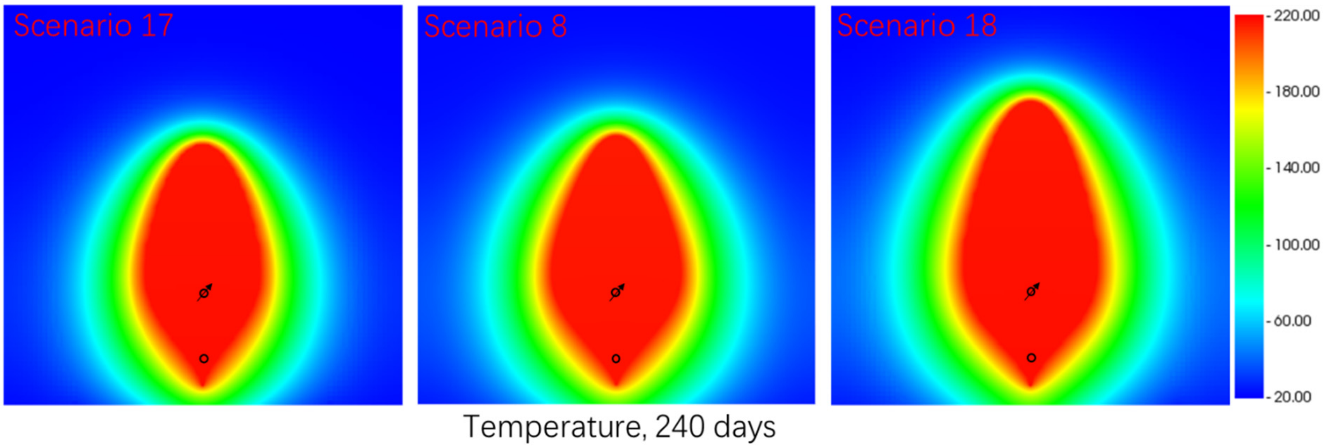

Figure 16. Cross-sectional temperature distributions of scenarios 8, 17 and 18 under varying initial water saturation.

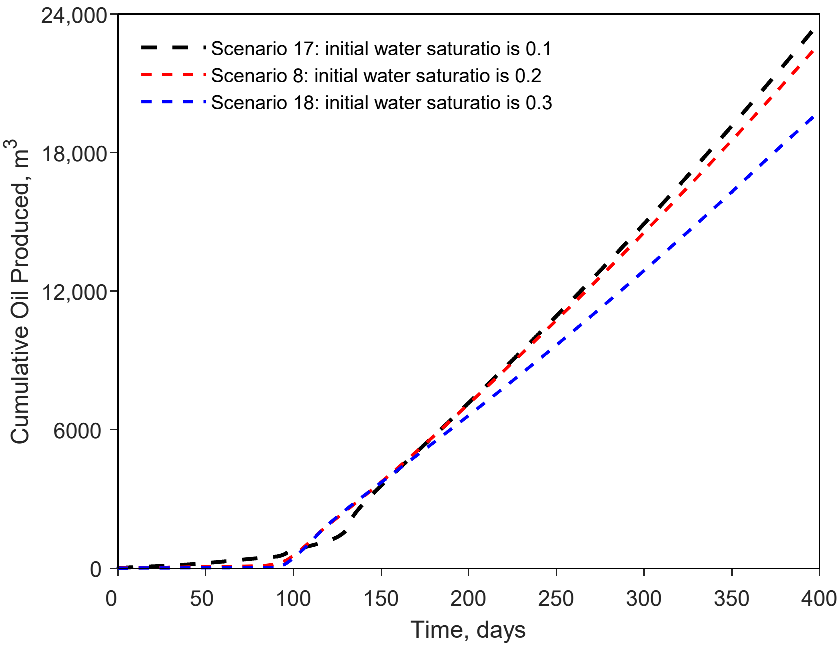

Figure 17. Cumulative oil production of scenarios 8, 17 and 18 under varying initial water saturation.

6. Conclusions

The dynamics of the SAGD steam chamber ramp-up phase were examined using a detailed thermal reservoir simulation model. The conclusions from the research are as follows:

1. A reliable and efficient numerical reservoir simulation model was generated for the modeling of the steam chamber ramp-up phase in an SAGD process using the application of dynamic gridding that was based on a fine grid simulation model;

2. The steam chamber ramp-up phase of SAGD is a complex process and the temperature-dependent multiphase flow and vertical countercurrent flow were essential parameters for the estimation of the ramp-up phase. The countercurrent flow slowed down the vertical growth of the steam chamber and essentially eliminated the effects of the temperature-dependent multiphase flow on the steam chamber ramp-up phase;
3. In an SAGD ramp-up phase, it was found that the countercurrent flow was the dominant multiphase flow pattern, over the cocurrent flow, in terms of the growth of the vertical steam chamber;
4. The initial water satiation altered the steam chamber ramp-up phase once the saturation was higher than the connate water saturation under the injected steam temperature conditions.

Author Contributions: Conceptualization, D.J. and Z.L.; methodology, D.J.; software, X.L.; validation, D.J.; formal analysis, J.Z.; investigation, J.X.; resources, J.X.; data curation, J.X.; writing—original draft preparation, D.J.; writing—review and editing, Z.L.; visualization, X.L.; supervision, Z.L.; project administration, D.J.; funding acquisition, D.J and J.Z. All authors have read and agreed to the published version of the manuscript.

Funding: This research was funded by CNPC Innovation Fund, grant number 2020D-5007-0204, and the Youth Project of the National Natural Science Foundation of China, grant number 52004219.

Institutional Review Board Statement: Not applicable.

Informed Consent Statement: Not applicable.

Data Availability Statement: Not applicable.

Conflicts of Interest: The authors declare no conflict of interest. The funders had no role in the design of the study, the collection, analyses or interpretation of the data, the writing of the manuscript or the decision to publish the results.

References

1. Butler, R.; Stephens, D. The Gravity Drainage of Steam-heated Heavy Oil to Parallel Horizontal Wells. *J. Can. Pet. Technol.* **1981**, *20*, 90–96. [CrossRef]
2. Edmunds, N. On the Difficult Birth of SAGD. *J. Can. Pet. Technol.* **1999**, *38*, 14–17. [CrossRef]
3. Komery, D.; Luhning, R.; O'Rourke, J. Towards Commercialization of the UTF Project Using Surface Drilled Horizontal SAGD Wells. *J. Can. Pet. Technol.* **1999**, *38*, 36–43. [CrossRef]
4. Butler, R. Rise Of Interfering Steam Chambers. *J. Can. Pet. Technol.* **1987**, *26*, 70–75. [CrossRef]
5. Gates, I.D.; Leskiw, C. Impact of steam trap control on performance of steam-assisted gravity drainage. *J. Pet. Sci. Eng.* **2010**, *75*, 215–222. [CrossRef]
6. Butler, R.M. *Thermal Recovery of Oil and Bitumen*, 3rd ed.; Grav Drain Inc.: Calgary, AB, Canada, 1997.
7. Gallardo, E.C.; Deutsch, C.V. Approximate Physics-Discrete Simulation of the Steam-Chamber Evolution in Steam-Assisted Gravity Drainage. *SPE J.* **2019**, *24*, 477–491. [CrossRef]
8. Chung, K.; Butler, R. Geometrical Effect Of Steam Injection On The Formation Of Emulsions Nn The Steam-Assisted Gravity Drainage Process. *J. Can. Pet. Technol.* **1988**, *27*, 36–42. [CrossRef]
9. Edmunds, N.R.; Kovalsky, J.A.; Gittins, S.D.; Pennacchioli, E.D. Review of Phase A Steam-Assisted Gravity-Drainage Test. *SPE Reserv. Eng.* **1994**, *9*, 119–124. [CrossRef]
10. Zhu, L.; Zeng, F. A Condensation Heating Model for Evaluating Early-Period SAGD Performance. *Transp. Porous Media* **2014**, *104*, 363–383. [CrossRef]
11. Li, P.; Chan, M.; Froehlich, W. Steam Injection Pressure and the SAGD Ramp-Up Process. *J. Can. Pet. Technol.* **2009**, *48*, 36–41. [CrossRef]
12. Irani, M. Oil-Rate Prediction Model for the Ramp-Up Phase of a Steam-Assisted-Gravity-Drainage Process: Stability Approach. *SPE J.* **2019**, *24*, 1016–1036. [CrossRef]
13. Keshavarz, M.; Harding, T.G.; Chen, Z. A New Approach to the Analytical Treatment of Steam-Assisted Gravity Drainage: A Prescribed Interface Model. *SPE J.* **2019**, *24*, 492–510. [CrossRef]
14. Reis, J.C. A Steam-Assisted Gravity Drainage Model For Tar Sands: Linear Geometry. *J. Can. Pet. Technol.* **1992**, *31*, 14–20. [CrossRef]
15. Ito, Y.; Ipek, G. Steam Fingering Phenomenon During SAGD Process. Presented at the SPE International Thermal Operations and Heavy Oil Symposium, Calgary, AB, Canada, 1–3 November 2005. [CrossRef]

16. Keshavarz, M.; Harding, T.G.; Chen, Z.J. Modification of Butler's Unsteady-State SAGD Theory to Include the Vertical Growth of Steam Chamber. Presented at the SPE Canada Heavy Oil Technical Conference, Calgary, AB, Canada, 7–9 June 2016. [CrossRef]
17. Zargar, Z.; Ali, S.F. Analytical modelling of steam chamber rise stage of Steam-Assisted Gravity Drainage (SAGD) process. *Fuel* **2018**, *233*, 732–742. [CrossRef]
18. Irani, M.; Ghannadi, S. Understanding the Heat-Transfer Mechanism in the Steam-Assisted Gravity-Drainage (SAGD) Process and Comparing the Conduction and Convection Flux in Bitumen Reservoirs. *SPE J.* **2013**, *18*, 134–145. [CrossRef]
19. Esmaeili, S.; Modaresghazani, J.; Sarma, H.; Harding, T.; Maini, B. Effect of temperature on relative permeability—Role of viscosity ratio. *Fuel* **2020**, *278*, 118318. [CrossRef]
20. Nakornthap, K.; Evans, R.D. Temperature-Dependent Relative Permeability and Its Effect on Oil Displacement by Thermal Methods. *SPE Reserv. Eng.* **1986**, *1*, 230–242. [CrossRef]
21. Maini, B.; Okazawa, T. Effects Of Temperature On Heavy Oil-Water Relative Permeability Of Sand. *J. Can. Pet. Technol.* **1987**, *26*, 33–41. [CrossRef]
22. Schembre, J.M.; Tang, G.-Q.; Kovscek, A.R. Interrelationship of Temperature and Wettability on the Relative Permeability of Heavy Oil in Diatomaceous Rocks. *SPE Reserv. Eval. Eng.* **2006**, *9*, 239–250. [CrossRef]
23. Akhlaghinia, M.; Torabi, F.; Chan, C.W. Experimental investigation of temperature effect on three-phase relative permeability isoperms in heavy oil systems. *Fuel* **2014**, *118*, 281–290. [CrossRef]
24. Zeidani, M.; Maini, B.B. SAGD Relative Permeability as A Function of Temperature. Presented at the SPE Canada Heavy Oil Technical Conference, Calgary, AB, Canada, 7–9 June 2016. [CrossRef]
25. Doranehgard, M.H.; Siavashi, M. The effect of temperature dependent relative permeability on heavy oil recovery during hot water injection process using streamline-based simulation. *Appl. Therm. Eng.* **2018**, *129*, 106–116. [CrossRef]
26. Esmaeili, S.; Sarma, H.; Harding, T.; Maini, B. Two-phase bitumen/water relative permeability at different temperatures and SAGD pressure: Experimental study. *Fuel* **2020**, *276*, 118014. [CrossRef]
27. Esmaeili, S.; Sarma, H.; Harding, T.; Maini, B. Experimental Study of the Effect of Solvent Addition and Temperature on Two-Phase Bitumen/Water Relative Permeability. *SPE Reserv. Eval. Eng.* **2020**, *23*, 1381–1402. [CrossRef]
28. Esmaeili, S.; Sarma, H.; Harding, T.; Maini, B. A data-driven model for predicting the effect of temperature on oil-water relative permeability. *Fuel* **2019**, *236*, 264–277. [CrossRef]
29. Esmaeili, S.; Sarma, H.; Harding, T.; Maini, B. Review of the effect of temperature on oil-water relative permeability in porous rocks of oil reservoirs. *Fuel* **2019**, *237*, 91–116. [CrossRef]
30. Esmaeili, S.; Sarma, H.; Harding, T.; Maini, B. Correlations for effect of temperature on oil/water relative permeability in clastic reservoirs. *Fuel* **2019**, *246*, 93–103. [CrossRef]
31. Torabi, F.; Mosavat, N.; Zarivnyy, O. Predicting heavy oil/water relative permeability using modified Corey-based correlations. *Fuel* **2016**, *163*, 196–204. [CrossRef]
32. Zhang, L.-H.; Tong, J.; Xiong, Y.; Zhao, Y.-L. Effect of temperature on the oil-water relative permeability for sandstone reservoirs. *Int. J. Heat Mass Transf.* **2017**, *105*, 535–548. [CrossRef]
33. Ji, D.; Wu, S.; Wang, B.; Li, Z.; Lai, F.; Chen, Z.; Dong, M.; Ge, C. Temperature-Dependent Irreducible Water Trapping in Heavy-Oil Reservoirs. *SPE J.* **2021**, *26*, 2245–2270. [CrossRef]
34. Li, S.; Li, Z. Effect of Temperature on the Gas/Oil Relative Permeability of Orinoco Belt Foamy Oil. *SPE J.* **2016**, *21*, 170–179. [CrossRef]
35. Guo, Y.; Liu, H.; Feng, Y.; Dong, X.; Zheng, W. A new SAGD comprehensive multi-stage model for oil production using a concave parabola geometry. *J. Pet. Sci. Eng.* **2021**, *208*, 109321. [CrossRef]
36. Butler, R. Steam-Assisted Gravity Drainage: Concept, Development, Performance And Future. *J. Can. Pet. Technol.* **1994**, *33*, 44–50. [CrossRef]
37. Nasr, T.; Law, D.; Golbeck, H.; Korpany, G. Counter-current Aspect of the SAGD Process. *J. Can. Pet. Technol.* **2000**, *39*, 41–47. [CrossRef]
38. Bourbiaux, B.J.; Kalaydjian, F.J. Experimental Study of Cocurrent and Countercurrent Flows in Natural Porous Media. *SPE Reserv. Eng.* **1990**, *5*, 361–368. [CrossRef]
39. Eastwood, J.; Spanos, T. Steady-state countercurrent flow in one dimension. *Transp. Porous Media* **1991**, *6*, 173–182. [CrossRef]
40. Langaas, K.; Papatzacos, P. Numerical Investigations of the Steady State Relative Permeability of a Simplified Porous Medium. *Transp. Porous Media* **2001**, *45*, 241–266. [CrossRef]
41. Sherafati, M.; Jessen, K. Modeling and Simulation of WAG Injection Processes—The Role of Counter-Current Flow. Presented at the SPE Western Regional Meeting, Garden Grove, CA, USA, 27–30 April 2015. [CrossRef]
42. Babchin, A.J.; Nasr, T.N. Analytical Model for The Capillary Pressure Gradient in Oil–Water—Rock System. *Transp. Porous Media* **2006**, *65*, 359–362. [CrossRef]
43. Bentsen, R.G.; Manai, A.A. On the use of conventional cocurrent and countercurrent effective permeabilities to estimate the four generalized permeability coefficients which arise in coupled, two-phase flow. *Transp. Porous Media* **1993**, *11*, 243–262. [CrossRef]
44. Dullien, F.A.L.; Dong, M. Experimental determination of the flow transport coefficients in the coupled equations of two-phase flow in porous media. *Transp. Porous Media* **1996**, *25*, 97–120. [CrossRef]
45. Al-Bahlani, A.-M.; Babadagli, T. SAGD laboratory experimental and numerical simulation studies: A review of current status and future issues. *J. Pet. Sci. Eng.* **2009**, *68*, 135–150. [CrossRef]

46. Sasaki, K.; Satoshi, A.; Yazawa, N.; Kaneko, F. Microscopic Visualization with High Resolution Optical-Fiber Scope at Steam Chamber Interface on Initial Stage of SAGD Process. Presented at the SPE/DOE Improved Oil Recovery Symposium, Tulsa, Oklahoma, 13–17 April 2002. [CrossRef]
47. Yang, M.; Chai, M.; Qi, R.; Chen, Z.; Zhang, L.; Yu, X. Dimethyl Ether as a Novel Solvent for Bitumen Recovery: Mechanisms of Improved Mass Transfer and Energy Efficiency. *SPE J.* **2021**, *27*, 1321–1340. [CrossRef]
48. Ehrlich, R. The Effect of Temperature on Water—Oil Imbibition Relative Permeability. Presented at the SPE Eastern Regional Meeting, Pittsburgh, PA, USA, 5–6 November 1970. [CrossRef]
49. Picchi, D.; Battiato, I. Scaling of two-phase water-steam relative permeability and thermal fluxes in porous media. *Int. J. Multiph. Flow* **2020**, *129*, 103257. [CrossRef]
50. Mendoza, A.M.; Kantzas, A. Simulation of Non-condensable Gases Co-Injection in Steam Assisted Gravity Drainage: The Role of Gas-Liquid Relative Permeability Curves. Presented at the SPE Canada Heavy Oil Conference, Calgary, AB, Canada, 28 September–2 October 2020. [CrossRef]
51. Mendoza, A.M.; Kantzas, A. Simulation of Non-condensable Gases Co-injection in Steam Assisted Gravity Drainage: State of the Art and Important Mechanisms. Presented at the SPE Canada Heavy Oil Conference, Virtual, 28 September–2 October 2020. [CrossRef]
52. Yuan, J.; Coombe, D.; Law, D.; Babchin, A. Determination of the Relative Permeability Matrix Coefficients. In Proceedings of the Canadian International Petroleum Conference, Calgary, AB, Canada, 12–14 June 2001. [CrossRef]
53. CMG (Computer Modelling Group). *STARS Thermal Reservoir Simulator User Manual*; CMG (Computer Modelling Group): Newport Beach, CA, USA, 2020.
54. Yang, M.; Harding, T.G.; Chen, Z. Field-Scale Modeling of Hybrid Steam and In-Situ-Combustion Recovery Process in Oil-Sands Reservoirs Using Dynamic Gridding. *SPE Reserv. Eval. Eng.* **2020**, *23*, 311–325. [CrossRef]
55. Christensen, J.; Darche, G.; Dechelette, B.; Ma, H.; Sammon, P. Applications of Dynamic Gridding to Thermal Simulations. Presented at the SPE International Thermal Operations and Heavy Oil Symposium and Western Regional Meeting, Bakersfield, CA, USA, 16–18 March 2004. [CrossRef]
56. Ji, D.; Dong, M.; Chen, Z. Analysis of steam–solvent-bitumen phase behavior and solvent mass transfer for improving the performance of the ES-SAGD process. *J. Pet. Sci. Eng.* **2015**, *133*, 826–837. [CrossRef]
57. Zhu, L.; Zeng, F.; Huang, Y. A correlation of steam chamber size and temperature falloff in the early-period of the SAGD Process. *Fuel* **2015**, *148*, 168–177. [CrossRef]
58. Patel, K.; Aske, E.M.; Fredriksen, M. Use of Model-Predictive Control for Automating SAGD Well-Pair Operations: A Simulation Study. *SPE Prod. Oper.* **2014**, *29*, 105–113. [CrossRef]
59. Qiao, Y.; Andersen, P.; Evje, S.; Standnes, D. A mixture theory approach to model co- and counter-current two-phase flow in porous media accounting for viscous coupling. *Adv. Water Resour.* **2018**, *112*, 170–188. [CrossRef]
60. Ji, D.; Zhong, H.; Dong, M.; Chen, Z. Study of heat transfer by thermal expansion of connate water ahead of a steam chamber edge in the steam-assisted-gravity-drainage process. *Fuel* **2015**, *150*, 592–601. [CrossRef]
61. Doan, Q.T.; Ali, S.M.F.; Tan, T.B. SAGD Performance Variability—Analysis of Actual Production Data for 28 Athabasca Oil Sands Well Pairs. Presented at the SPE Western Regional Meeting, San Jose, CA, USA, 23–26 April 2019. [CrossRef]
62. Law, D.; Nasr, T.; Good, W. Field-Scale Numerical Simulation of SAGD Process With Top-Water Thief Zone. *J. Can. Pet. Technol.* **2003**, *42*, 32–38. [CrossRef]
63. Zhou, W.; Dong, M.; Chen, S. Investigation of initial water mobility and its effects on SAGD performance in bitumen reservoirs and oil sands. *J. Pet. Sci. Eng.* **2015**, *135*, 39–49. [CrossRef]
64. Ji, D.; Zhong, H.; Dong, M.; Chen, Z.; Jia, X. A Model to Estimate Heat Efficiency in Steam-Assisted Gravity Drainage by Condensate and Initial Water Flow in Oil Sands. *Ind. Eng. Chem. Res.* **2016**, *55*, 13147–13156. [CrossRef]